Psychometric functions of uncertain template matching observers

Wilson S. Geisler

Center for Perceptual Systems and Department of Psychology, University of Texas at Austin, Austin, TX, USA

This theoretical note describes a simple equation that closely approximates the psychometric functions of template-matching observers with arbitrary levels of position and orientation uncertainty. We show that the approximation is accurate for detection of targets in white noise, 1/f noise, and natural backgrounds. In its simplest form, this equation, which we call the uncertain normal integral (UNI) function, has two parameters: one that varies only with the level of uncertainty and one that varies only with the other properties of the stimuli. The UNI function is useful for understanding and generating predictions of uncertain template matching (UTM) observers. For example, we use the UNI function to derive a closed-form expression for the detectability (d') of UTM observers in 1/f noise, as a function of target amplitude, background contrast, and position uncertainty. As a descriptive function, the UNI function is just as flexible and simple as other common descriptive functions, such as the Weibull function, and it avoids some of their undesirable properties. In addition, the estimated parameters have a clear interpretation within the family of UTM observers. Thus, the UNI function may be the better default descriptive formula for psychometric functions in detection and discrimination tasks.

Introduction

Many different descriptive functions have been used to summarize psychometric data measured in detection and discrimination experiments. The common functions include the normal integral function, the logistic function, and the Weibull function. This theoretical note proposes a descriptive function that is based on the principles of detection under stimulus uncertainty. The simplest form of this function is as follows:

$$F(x) = \Phi\left[\frac{1}{2}\ln\left(\frac{e^{\alpha x}+\beta}{1+\beta}\right)\right] \quad x \geq 0 \quad (1)$$

where x is the value of stimulus property being varied, α and β are constants, and $\Phi(\cdot)$ is the standard normal integral function. This function will be referred to here as the uncertain normal integral (UNI) function. Here, we demonstrate with simulations that the UNI function provides a close approximation to the psychometric functions of template-matching observers in white noise, 1/f noise, and natural backgrounds, for arbitrary levels of uncertainty about target position and orientation (and probably other dimensions of signal variation). The parameter β varies only with the level of uncertainty. The parameter α depends on the other properties of the stimuli, but does not vary with level of uncertainty. Thus, in the absence of observer uncertainty, the UNI function reduces to a normal integral function with a standard deviation of $2/\alpha$. We argue that the UNI function (a) is useful for characterizing and computing the predictions of template matching observers with uncertainty, (b) avoids practical and conceptual problems that sometimes arise with the other descriptive functions, and (c) may provide a more principled interpretation of psychometric data.

Uncertain template matching (UTM) observers

Template matching observers are a well-known family of models of detection and discrimination. In detection and discrimination tasks, a stimulus from one of two possible categories, a and b, is presented on each trial. In the absence of uncertainty, a template matching observer computes the dot product of a template $f(x, y)$ with the input stimulus $I(x, y)$:

$$R = f \cdot I = \sum_{x,y} f(x,y)I(x,y) \quad (2)$$

The observer then compares the template response R to a decision criterion γ; if the response exceeds the criterion, then the observer responds that the stimulus was from category b, otherwise that it was from category a. In the case of detection in a background of Gaussian white noise, the stimulus from category a is a sample of white noise, and the stimulus from category b is a sample of white noise with an added target of some

Citation: Geisler, W. S. (2018). Psychometric functions of uncertain template matching observers. *Journal of Vision*, *18*(2):1, 1–10, https://doi.org/10.1167/18.2.1.

https://doi.org/10.1167/18.2.1 Received September 26, 2017; published February 1, 2018 ISSN 1534-7362

amplitude. If the observer's template has the same shape as the target, then the observer's accuracy will be the highest possible in this task (Peterson, Birdsall, & Fox, 1954; Green & Swets, 1974; Burgess, Wagner, Jennings, & Barlow, 1981; Geisler, 2011).

If the observer's template has a different shape or if the template has the same shape and the background noise is not white, then performance will be suboptimal.

If the template matching observer is uncertain, the observer applies the template over the region of uncertainty Ω, computes the maximum of the template responses

$$R = \max_{\omega \in \Omega} f_\omega \cdot I \quad (3)$$

and then compares that maximum response to a decision criterion γ (e.g., Nolte & Jaarsma, 1967; Swensson & Judy, 1981; Shaw, 1982; Pelli, 1985). If the observer is uncertain about the position of the target, then Ω is the set of potential target locations, $\boldsymbol{\omega} = (x, y)$; if uncertain about the orientation of the target, then Ω is the set of potential target orientations, $\boldsymbol{\omega} = \theta$; and so on. Again, if the background is Gaussian white noise, the template has the shape of the target, and the uncertainty region corresponds to the actual range of variation of the target, then the uncertain template matching (UTM) observer will perform close to the optimal possible in the task (Peterson et al., 1954; Tanner, 1961; Nolte & Jaarsma, 1967; Shaw, 1982; Pelli, 1985; see later in this article). Of course, more biologically plausible UTM observers may have non-optimal templates and intrinsic uncertainty. However, our primary concern here is with the performance of UTM observers independent of whether they are optimal or not. In other words, the aim is to demonstrate that Equation 1 accurately describes the psychometric functions of UTM observers.

In the signal detection theory framework (Green & Swets, 1974), the performance of an observer in a two-alternative detection or discrimination experiment is described by two numbers, the discriminability d' and the decision criterion γ. The discriminability represents the intrinsic ability of the observer to perform the task, and the decision criterion any potential bias. For now we assume that the two stimulus categories are presented with equal probability, and that the UTM observer's criterion is always set to the optimal value (no bias). The effect of bias is easy to include. For equal presentation probabilities and no bias, an observer's accuracy is given by

$$F(x) = \Phi\left[\frac{d'(x)}{2}\right] \quad (4)$$

Thus, from Equation 1 we see that the UNI function expressed in d' units is

$$d'(x) = \ln\left(\frac{e^{\alpha x} + \beta}{1 + \beta}\right) \quad x \geq 0 \quad (5)$$

The symbols in Figure 1 show d' values of the UTM observer for detection of a raised-cosine-widowed sinewave target in Gaussian white noise, in a single interval identification ("Yes-No") task. The target was 17 pixels in diameter and had a frequency of 1/8 cy/pixel. Each point is based on 2000 simulated trials. In computing the UTM observer's d' values, we applied the following formula to the sampled means and variances:

$$d' = \frac{[\text{mean}(R|b) - \text{mean}(R|a)]\sqrt{2}}{\sqrt{\text{var}(R|b) + \text{var}(R|a)}} \quad (6)$$

A slightly better approximation to the UTM observer's d' values is given in the Appendix; however, using that approximation does not affect the quality of the UNI function predictions or any of the conclusions (see later).

Each panel in Figure 1 is for a different radius of position uncertainty around the center pixel of the target. For example, when the uncertainty radius is 32 pixels, the UMT observer computes the template response at each of $\pi 32^2 = 3{,}217$ pixel locations and then selects the maximum. The different colored symbols represent different root-mean-squared (RMS) contrast levels for the noise background. The curves in the plot show the minimum squared-error fit of Equation 5. For each value of background contrast (colors) the parameter α is fixed, and for each uncertainty radius (panels) the parameter β is fixed (the α values and single β value in a panel were estimated simultaneously). Clearly, the UNI function provides a close approximation to the performance of the simulated UTM observer. The approximation remains close at other values of uncertainty, noise contrast, and target amplitude. Not surprisingly, the fits look equally good when plotted in units of proportion correct (Equation 1). For example, Figure 2 is a replot of the simulations and fits in Figure 1C.

Gaussian white noise is popular as a background in psychophysical experiments. This popularity is largely due to the fact that it is spatially uncorrelated, which greatly simplifies mathematical modeling and analysis of the psychophysical data. However, the backgrounds that occur under natural conditions are spatially correlated. Gaussian 1/f noise has the power spectrum of natural images (Burton & Moorehead, 1987; Field, 1987), and hence contains some of the spatial correlations that occur under natural conditions. Gaussian 1/f noise is also popular because it is precisely specified, naturalistic, and relatively tractable for modeling and analysis. How do the spatial correlations in 1/f noise affect the performance of the UTM observers and the accuracy of the UNI function

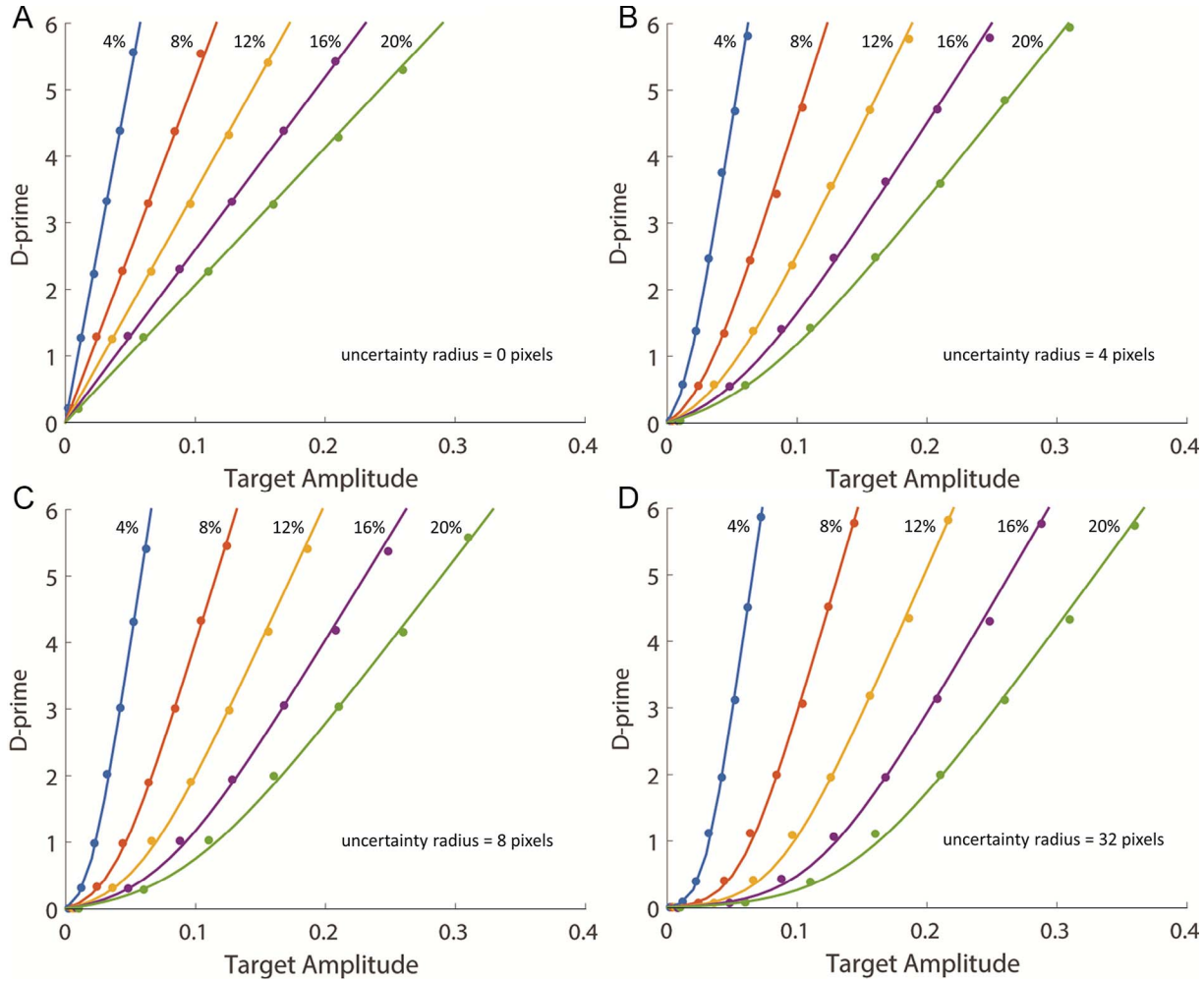

Figure 1. Detectability (d') of the uncertain template matching (UTM) observer as a function of target amplitude, for a windowed sinewave target in Gaussian white noise. The color indicates the RMS contrast (in percent) of the noise background. Each panel is for a different level of position uncertainty. Each data point is the UTM observer's performance on 2,000 simulated trials. The curves are the best fitting UNI function in d' units (Equation 5). The parameter α is fixed for each level of noise contrast, and the parameter β is fixed for each level of uncertainty.

approximation? The circles in Figure 3 show the simulated detectabilities of the UTM observer for the same windowed sinewave target, uncertainties, and background contrasts used with the white noise backgrounds. Because of the spatial correlations, the detectabilities in 1/f noise are lower than white noise (note change of axes); however, the solid curves show that the fit of the UNI function is just as accurate as in white noise.

The approximation also remains good for other targets. For example, Figure 4 shows (for 1/f noise) simulations and fits for a raised-cosine target (full width = 17 pixels), which is a broadband target with nonzero mean. Although the fit is just as good as for the windowed sinewave target, the amplitude of the target must be higher to reach the same levels of detectability (note the different x axis scales in Figures 3 and 4).

The UNI function also provides a good approximation when the uncertainty is in orientation rather than position, although the effects of orientation uncertainty are smaller. Figure 5 shows simulation and fits for detection of the windowed sinewave target for the cases of no uncertainty and uniform orientation uncertainty over the range ±89°.

In addition to simulations with noise backgrounds, simulations were run with background patches randomly sampled from natural images. The natural image patches were binned along the dimensions of mean luminance, RMS contrast, and cosine similarity between the amplitude spectrum of the background and a windowed sinewave target (see Sebastian et al., 2017 for details). For this simulation, all the image patches were randomly drawn from the same bin (e.g., they all had the same contrast, mean luminance, and cosine similarity). The symbols in Figure 6 plot the

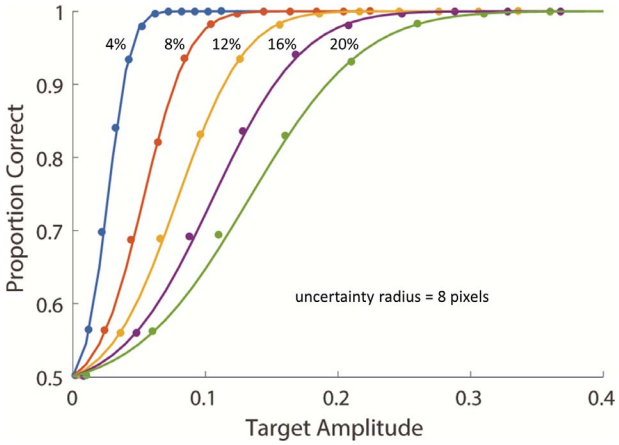

Figure 2. Replot of Figure 1C in units of proportion correct rather than detectability. Data points are simulations. The solid curves are the predictions (Equation 1).

detectability of the UTM observer as function of target amplitude for several levels of position uncertainty. The solid curves are the best fitting UNI functions (Equation 5). Thus, even for natural backgrounds the UNI function provides a good approximation.

The symbols in Figure 7 plot the thresholds of the UTM observer in 1/f noise for a range of background contrasts and levels of position uncertainty. The straight lines in Figure 7 are the predictions of Weber's law, which holds accurately for all levels of uncertainty. Setting $d' = 1.0$ in Equation 5, we see that the threshold of the UTM observer is given by

$$a_t = \ln[e + (e-1)\beta]/\alpha \quad (7)$$

When there is no uncertainty this equation reduces to

$$a_t = 1/\alpha \quad (8)$$

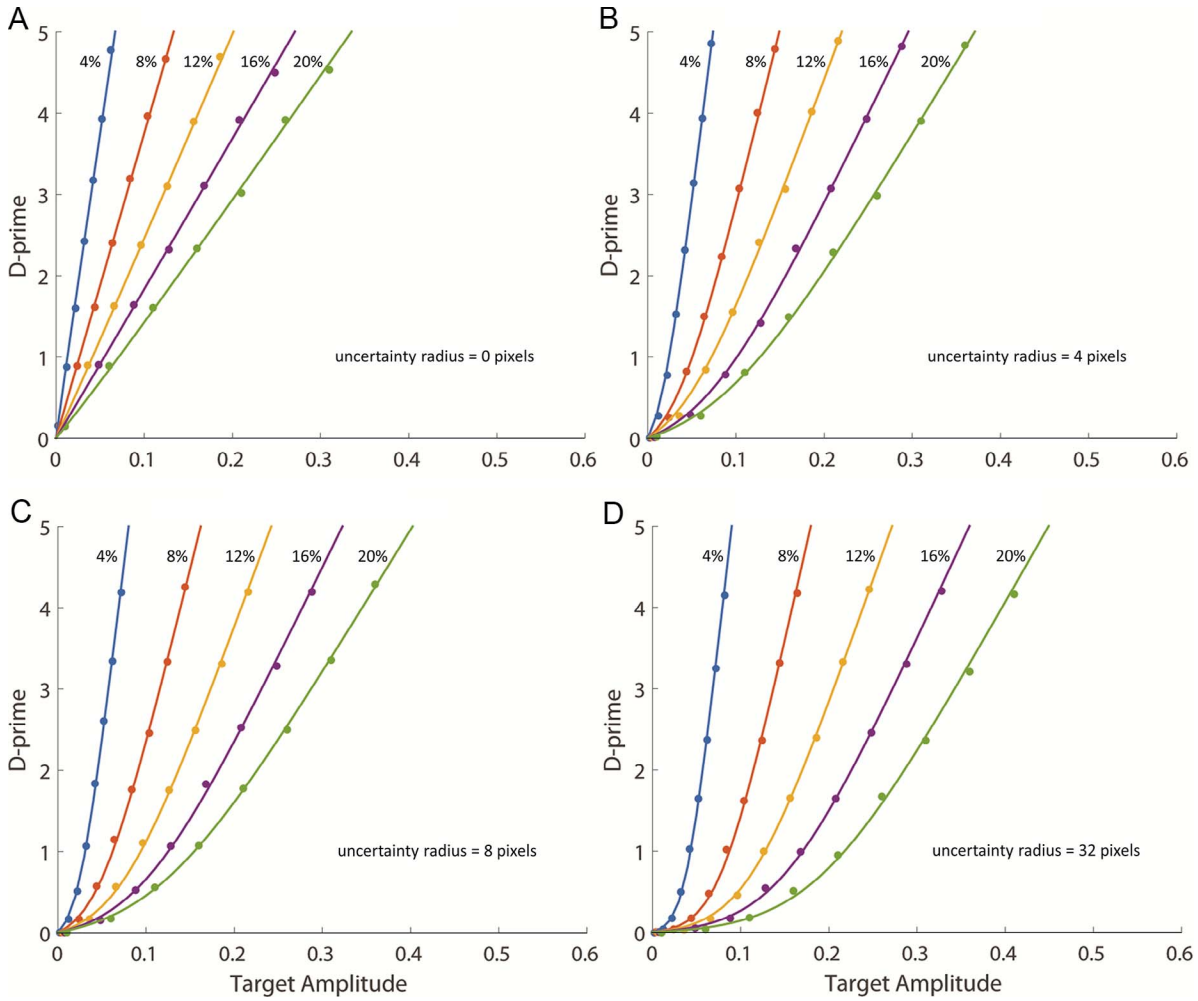

Figure 3. Detectability (d') of the UTM observer as a function of target amplitude, for a windowed sinewave target in Gaussian 1/f noise. The color indicates the RMS contrast (in percent) of the noise background. Each panel is for a different level of position uncertainty. Each data point is the UTM observer's performance on 2,000 simulated trials. The curves are the best fitting UNI function in d' units (Equation 5). The parameter α is fixed for each level of noise contrast, and the parameter β is fixed for each level of uncertainty.

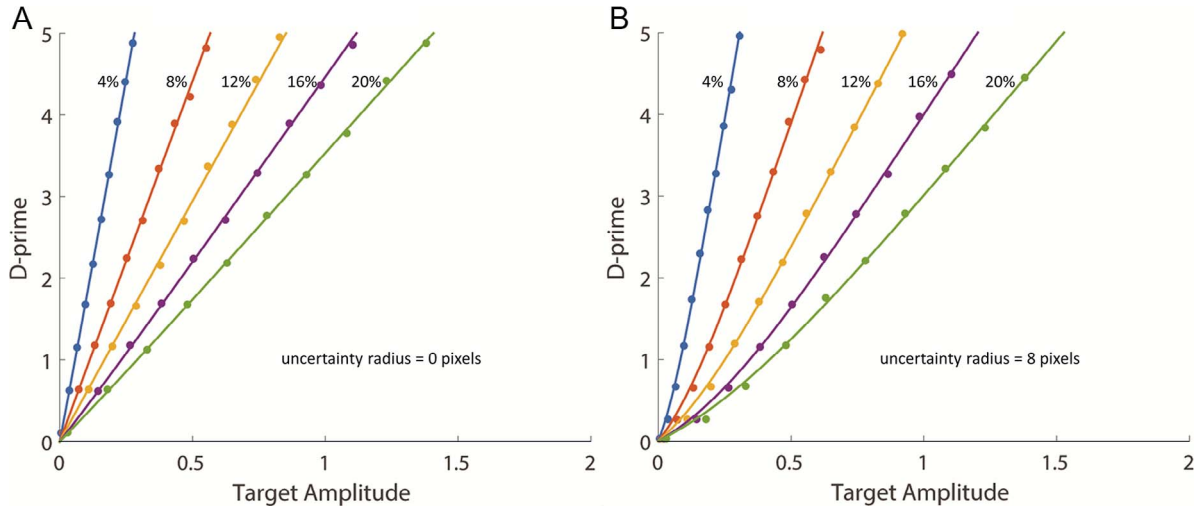

Figure 4. Detectability (d') of the UTM observer as a function of target amplitude, for a raised-cosine target (a blob). The color indicates the RMS contrast of the 1/f noise background. Each data point is the UTM observer's performance on 2,000 simulated trials. The curves are the best fitting UNI function in d' units (Equation 5).

Weber's law implies that without uncertainty

$$a_t = k_b c_b \quad (9)$$

where c_b is the background contrast and k_b is the slope of the masking function with 0 uncertainty (dark blue line in Figure 8; $k_b = 0.337$). It follows that

$$k_b c_b = 1/\alpha \quad (10)$$

and thus for arbitrary uncertainty that

$$a_t = \ln[e + (e-1)\beta] k_b c_b \quad (11)$$

If we divide the slope for each uncertainty level by k_b, we can determine how the relative slope of the masking function depends on the uncertainty radius. Figure 8 plots the relative slopes. The solid line in Figure 8 plots the predicted relative slope under the assumption that the uncertainty parameter β is proportional to the uncertainty radius r

$$\frac{m(r)}{m(0)} = \ln[e + (e-1)k_u r] \quad (12)$$

where m is the slope of the masking function, $k_u = 0.39$, and r is the uncertainty radius. Substituting into Equation 5 gives a closed-form approximation for the performance of the UTM observer (in this specific task, with this specific target) as a function of target

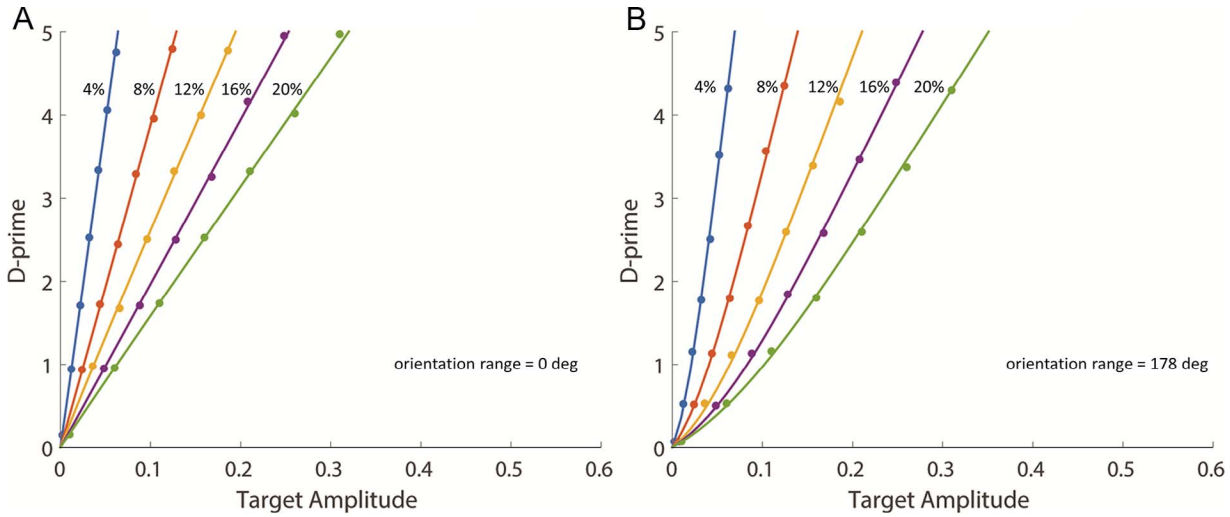

Figure 5. Detectability (d') of the UTM observer as a function of target amplitude, for a windowed sinewave target in 1/f noise. The color indicates the RMS contrast of the 1/f noise background. Each data point is the UTM observer's performance on 2,000 simulated trials. The two panels are for no uncertainty, and for an orientation uncertainty of $\pm$ 89°. The curves are the best fitting UNI function in d' units (Equation 5).

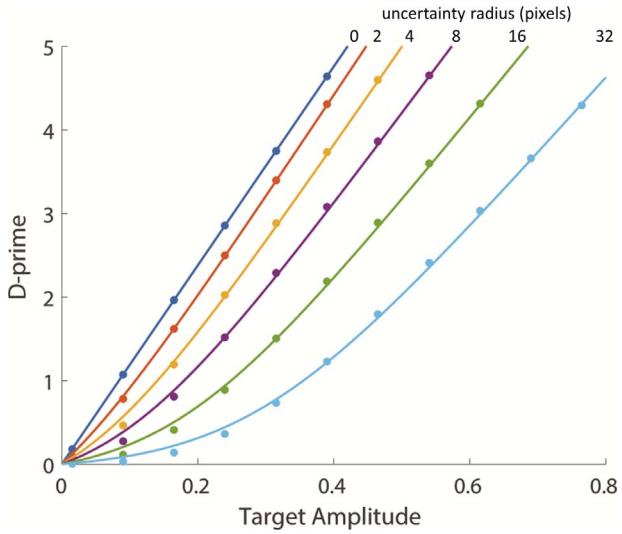

Figure 6. Detectability (d') of the UTM observer as a function of target amplitude, for a windowed sinewave target in natural backgrounds of contrast of 0.17 RMS and cosine similarity of 0.31, for several levels of target position uncertainty (for description of natural backgrounds see Sebastian et al., 2017).

amplitude, background contrast, and position uncertainty:

$$d'(x) = \ln\left(\frac{e^{\frac{x}{k_b c_b}} + k_u r}{1 + k_u r}\right) \quad x \geq 0 \quad (13)$$

This exercise demonstrates the potential usefulness of the UNI function for characterizing and understanding the predictions of UTM observer models.

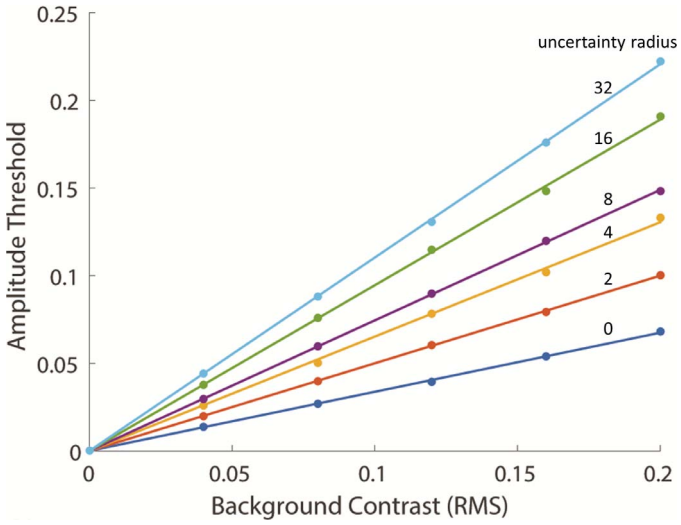

Figure 7. Amplitude threshold of the UTM observer as a function of background contrast and uncertainty radius, for a windowed sinewave target in 1/f noise. As expected, Weber's law holds for all levels of position uncertainty, with a Weber fraction that increases with the level of uncertainty.

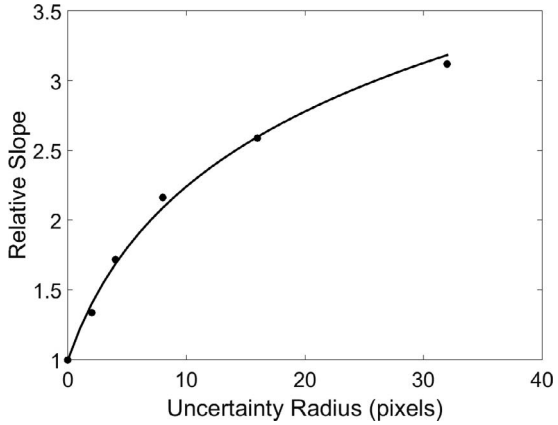

Figure 8. Relative slope of the contrast masking functions in Figure 8 for the different levels of position uncertainty. The solid curve is the prediction under the assumption that the uncertainty parameter β is proportional to the uncertainty radius r.

Comparison with other descriptive functions

As mentioned in the introduction many different functions have been used to summarize psychometric data in detection and discrimination experiments. Two that have been particularly popular are the Weibull function (Weibull, 1951; Quick, 1974; Graham, 1977)

$$F(x) = 1 - 0.5\exp\left[-(\alpha x)^{\beta}\right] \quad x \geq 0 \quad (14)$$

and the generalized normal integral (GNI) function (Nachmias & Sansbury, 1974; Foley & Legge, 1981)

$$F(x) = \Phi\left[\frac{1}{2}(\alpha x)^{\beta}\right] \quad x \geq 0 \quad (15)$$

Both of these functions are flexible enough to provide an adequate fit to psychometric data over the typical range of the independent variable (x) in psychophysical experiments. Also, they provide an adequate fit to the performance of UTM observers over a limited range. However, as Pelli (1985) notes, they fail over a broader range. Also, in some situations they make rather nonsensical predictions. For example, measurements of psychometric functions for detection in 1/f noise show that the steepness parameter β of the fitted functions tends to increase with retinal eccentricity (Najemnik & Geisler, 2005; Michel & Geisler, 2011). But, for both the Weibull and GNI function, this implies that detectability in the periphery will be better than in the fovea if the target amplitude is high enough (Figure 9B). In general, it seems very unlikely that supra-threshold objects in the periphery can have a bigger signal-to-noise ratio than in the fovea. With the UNI function it is possible to have steeper psychometric functions in the periphery without the detectability functions ever crossing (Figure 9A). Thus, there are

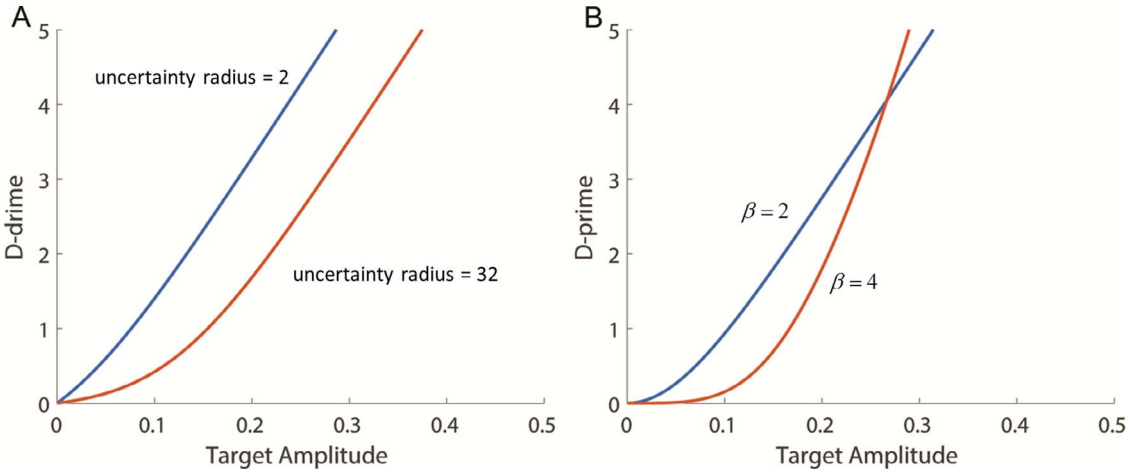

Figure 9. Comparison of UNI and Weibull functions. To mimic the effects of increased uncertainty on the psychometric function (e.g., more position uncertainty in the periphery than in the fovea), the exponent β of the Weibull function must increase. However, a steeper exponent implies that detectability under higher uncertainty must exceed that under lower uncertainty when the target amplitude becomes sufficiently high—a counterintuitive behavior.

cases (e.g., modeling visual search or differences between foveal or peripheral vision) where the UNI function may be more appropriate.

To account for curved d' psychometric functions, Lu and Dosher (1999, 2008) consider models with a nonlinear transducer plus sources of internal noise, rather than uncertainty. Such models can be designed so the d' psychometric functions do not cross, as in Figure 9A. However, these models have more parameters than the UNI function and do not include uncertainty. Below we note how the UNI function can be generalized to include all these factors.

Over limited ranges of detectability, the UNI function can approximate the Weibull (or GNI) function (and vice versa). Figure 10A shows the maximum likelihood fit of the UNI function (curves) to the Weibull psychometric function (points), over the range of steepness-parameter values (β) of the Weibull function that are typically observed in psychophysical studies. The parameter α simply scales the x axis of both functions so the fits are equally good for other values of α (Figure 10B). This figure demonstrates that the UNI function has similar flexibility for fitting psychometric function shapes.

A potential advantage of the UNI function is that its parameters have a meaningful interpretation within the family of uncertain template matching (UTM) observers. Recall that the parameter β is only affected by the

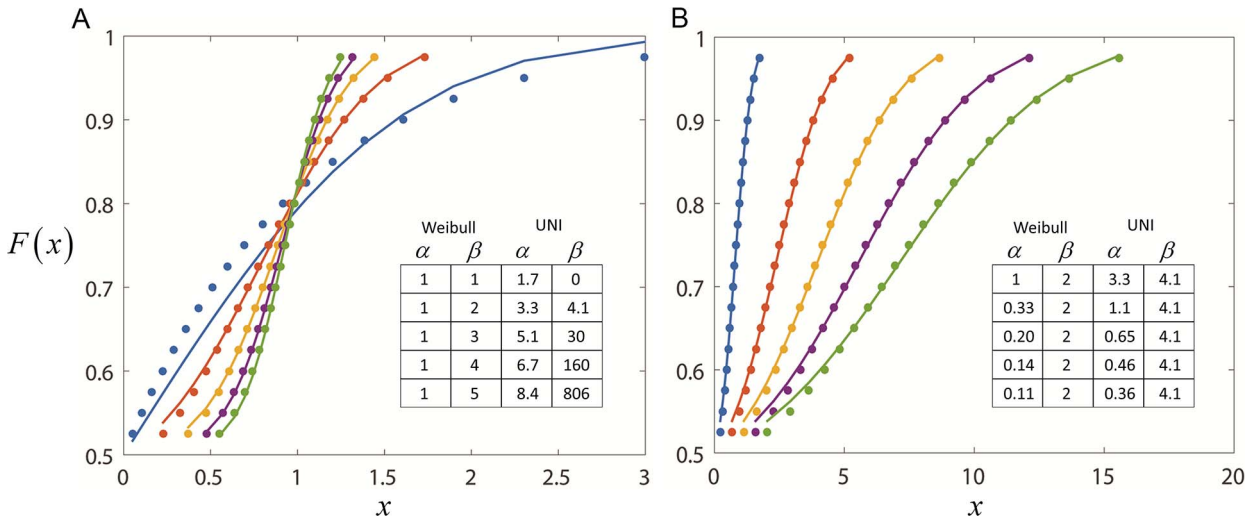

Figure 10. Comparison of Weibull psychometric functions (symbols) and UNI psychometric functions (curves) for probabilities ranging from 0.525 to 0.975. (A) Psychometric functions for different values of β and fixed value of α. (B) Psychometric functions for different values of α and a fixed value of β. The tables show the corresponding values of parameters for the two functions.

level of uncertainty and α only by the other properties of the backgrounds and targets. There is evidence that position and phase uncertainty are important factors limiting peripheral vision (Bennett & Banks, 1987; Hess & Hayes, 1994; Levi, 2008; Michel & Geisler, 2011). To the extent that intrinsic (and extrinsic) uncertainty plays a role in real performance, fitting the UNI function would provide an estimate of the effect of uncertainty, separate from the other factors affecting performance. Whether the estimated parameters of the UNI function will provide new insight into the mechanisms of visual performance and individual differences remains to be seen. But regardless, it is a principled descriptive function that is about as flexible and simple the Weibull or GNI function, and it avoids some of their nonintuitive properties. Thus, it would seem to be a better default descriptive formula for psychometric functions in detection and discrimination tasks.

Independent locations

The focus so far has been on the case of essentially continuous uncertainty about position or orientation over some region. This means that the template responses from the various locations are usually not statistically independent. However, a common case in experiments is when the uncertainty is over discrete nonoverlapping locations. In this case, the template responses are statistically independent. The circles in Figure 11 show simulations of detectability for the UTM observer in white noise, when there are 16 discrete nonoverlapping locations. In computing these detectabilities we used the slightly better approximation given in the Appendix (but as mentioned earlier, it has a minor effect). The solid curves show the simultaneous fit of the UNI function for a fixed value of the uncertainty parameter β and a different value of α for each background contrast level. We conclude that the UNI function works equally well for the case of statistically independent template responses.

For a description of the exact integral formulas for the max rule with independent noise, both for the current case, and the more general case of m-alternative forced choice tasks, see Eckstein et al. (1997).

Uncertain ideal observer

The UTM observer is simple and biologically plausible, but it is not the ideal observer under uncertainty. Rather than compute the max of the template responses (Equation 3), the ideal observer computes the likelihood ratio of the observed set of template responses under the assumptions that the target is present and absent,

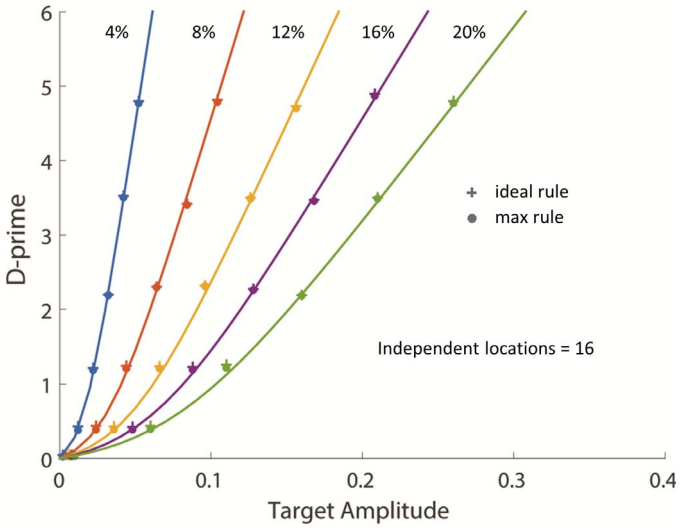

Figure 11. Detectability of the UTM (max rule) and ideal observer in white noise, for the case of 16 potential nonoverlapping locations of the target. Solid curves are the fit of the UNI function for a fixed uncertainty parameter β.

$$L = \frac{p(f_1 \cdot I, \cdots, f_m \cdot I|b)}{p(f_1 \cdot I, \cdots, f_m \cdot I|a)} \quad (16)$$

and then compares that likelihood ratio to the ratio of the prior probabilities of target absent and present. As mentioned earlier, for white noise the max rule performs almost as well as the ideal rule. This is demonstrated by the plus symbols in Figure 11, which are very slightly higher than the circles. (Note that the UNI function parameters would be slightly different if fit to the plus symbols.)

Generalizations of the UNI function

The UNI function can be generalized in various ways. For example, it is possible to generalize the function so that it can fit psychometric data where proportions vary from 0 to 1, and x can take values around some arbitrary value u (e.g., discrimination of leftward and rightward motion):

$$F(x) = \begin{cases} \Phi\left[\frac{1}{2}\ln\left(\frac{e^{\alpha(x-u)}+\beta}{1+\beta}\right)\right] & x \geq u \\ \Phi\left[-\frac{1}{2}\ln\left(\frac{e^{-\alpha(x-u)}+\beta}{1+\beta}\right)\right] & x < u \end{cases} \quad (17)$$

Also, it is simple to include a lapse rate parameter, which is often needed for animal and infant studies:

$$F(x) = (1-2\lambda)\Phi\left[\frac{1}{2}\ln\left(\frac{e^{\alpha x}+\beta}{1+\beta}\right)\right] + \lambda \quad x \geq 0 \quad (18)$$

where λ is the lapse rate.

Because the parameter β captures all the effects of uncertainty, the formula can be generalized fairly easily to allow nonlinear and noisy template matching. This generalization involves additional parameters, so this may not be appropriate for simply summarizing psychometric functions and estimating thresholds, but it could be useful for developing and testing models. Specifically, let the model's d' psychometric function for the case of no position or orientation uncertainty be $\psi(x)$. Then, the psychometric function in the case of position or orientation uncertainty becomes

$$F(x) = \Phi\left[\frac{1}{2}\ln\left(\frac{e^{\psi(x)}+\beta}{1+\beta}\right)\right] \quad x \geq 0 \quad (19)$$

We have not yet explored this family of psychometric functions, but it should include useful cases.

Keywords: psychometric function, uncertainty, template matching, masking

Acknowledgments

I thank Denis Pelli for helpful comments. This work was supported by NIH grants EY024662 and EY11747.

Commercial relationships: none.
Corresponding author: Wilson S. Geisler.
Email: w.geisler@utexas.edu.
Address: Center for Perceptual Systems and Department of Psychology, University of Texas at Austin, Austin, TX, USA.

References

Bennett, P. J., & Banks, M. S. (1987). Sensitivity loss in odd-symmetric mechanisms and phase anomalies in peripheral vision, *Nature*, *326*, 873–876, doi:10.1038/326873a0.

Burgess, A. E., Wagner, R. F., Jennings, R. J., & Barlow, H. B. (1981). Efficiency of human signal discrimination, *Science*, *214*, 93–94.

Burton, G. J., & Moorehead, I. R. (1987). Color and spatial structure in natural scenes. *Applied Optics*, *26*, 157–170.

Field, D. J. (1987). Relations between the statistics of natural images and the response properties of cortical cells. *Journal of the Optical Society of America A*, *4*, 2379–2394.

Foley, J. M., & Legge, G. E. (1981). Contrast detection and near-threshold discrimination in human vision. *Vision Research*, *21*, 1041–1053.

Geisler, W. S. (2011). Contributions of ideal observer theory to vision research. *Vision Research*, *51*, 771–781.

Graham, N. (1977). Visual detection of aperiodic stimuli by probability summation among narrow band channels. *Vision Research 17*, 637–652.

Green, D. M., & Swets, J. A. (1974). *Signal detection theory and psychophysics*. Huntington, NY: R. E. Krieger Publishing.

Hess, R. F., & Hayes, A. (1994). The coding of spatial position by the human visual system: Effects of spatial scale and retinal eccentricity. *Vision Research*, *34*, 625–643.

Levi, D. M. (2008). Crowding—An essential bottleneck for object recognition: A mini-review. *Vision Research*, *48*, 635–654.

Lu, Z. L., & Dosher, B. A. (1999). Characterizing human perceptual inefficiencies with equivalent internal noise. *Journal of the Optical Society of America A*, *16*, 764–778.

Lu, Z. L., & Dosher, B. A. (2008). Characterizing observers using external noise and observer models: Assessing internal representations with external noise, *Psychological Review*, *115*, 44–82.

Michel, M., & Geisler, W. S. (2011). Intrinsic position uncertainty explains detection and localization performance in peripheral vision. *Journal of Vision*, *11*(1):18, 1–18, doi:10.1167/11.1.18. [PubMed] [Article]

Nachmias, J., & Sansbury, R. V. (1974). Grating contrast discrimination may be better than detection. *Vision Research*, *14*, 1039–1042.

Najemnik, J., & Geisler, W. S. (2005). Optimal eye movement strategies in visual search. *Nature*, *434*, 387–391.

Nolte, L. W., & Jaarsma, D. (1967). More on the detection of one of M orthogonal signals. *Journal of the Acoustical Society of America*, *41*, 497–505.

Pelli, D. G. (1985). Uncertainty explains many aspects of visual contrast detection and discrimination. *Journal of the Optical Society of America A*, *2*, 1508–1532.

Peterson, W., Birdsall, T., & Fox, W. (1954). The theory of signal detectability. *IEEE Transactions on Information Theory*, *4*, 171–212.

Quick, R. F. (1974). A vector-magnitude model of contrast detection. *Kybernetik 16*, 65–67.

Sebastian, S., Abrams, J., & Geisler, W. S. (2017). Constrained sampling experiments reveal principles of detection in natural scenes. *Proceedings of the National Academy of Sciences*, *14*(28), E5731–E5740.

Shaw, M. L. (1982). Attending to multiple sources of

information: I. The integration of information in decision making, *Cognitive Psychology*, *14*, 353–409.

Swensson, R. G., & Judy, P. F. (1981). Detection of noisy visual targets: Models for the effects of spatial uncertainty and signal-to-noise ratio. *Perception & Psychophysics*, *29*, 521–534

Tanner, W. (1961). Physiological implications of psychophysical data. *Annals of the New York Academy of Sciences*, *89*, 752–765.

Weibull, W. (1951). A statistical distribution function of wide applicability. *Journal of Applied Mechanics 18*, 293–297.

Appendix

In general, the standard deviations of UTM observers' responses for the two stimulus categories are not equal. For example, Figure A1 shows the target-present and target-absent histograms of the UTM observer in 1/f noise, for a target whose amplitude is suprathreshold, when there is a high level of uncertainty (uncertainty radius of 32 pixels). In such cases, a better approximation than Equation 6 for the detectability is to (a) assume normal distributions with unequal variance, (b) set the criterion at the cross point between the two distributions, (c) compute the percent correct, and then (d) calculate the equivalent detectability from this percent correct. The percent correct is given by

$$PC = \frac{1}{2}\left[\Phi\left(\frac{u_b - \gamma}{\sigma_b}\right) + \Phi\left(\frac{\gamma - u_a}{\sigma_a}\right)\right] \quad \text{(A1)}$$

where u_a, u_b, σ_a, and σ_b are the means and standard deviations of the two distributions and γ is a decision criterion located at the cross point between the two distributions. Assuming $u_b > u_a$, the criterion is given by

$$\gamma = \frac{-B - \sqrt{B^2 - 4AC}}{2A} \quad \text{(A2)}$$

where,

$$A = \left(\frac{1}{2\sigma_b^2} - \frac{1}{2\sigma_a^2}\right),\ B = \left(\frac{u_a}{\sigma_a^2} - \frac{u_b}{\sigma_b^2}\right),\ \text{and}$$

$$C = \frac{u_b^2}{2\sigma_b^2} - \frac{u_a^2}{2\sigma_a^2} + \ln\frac{\sigma_b}{\sigma_a}.$$

The equivalent detectability is given by

$$d'_{eq} = 2\Phi^{-1}(PC) \quad \text{(A3)}$$

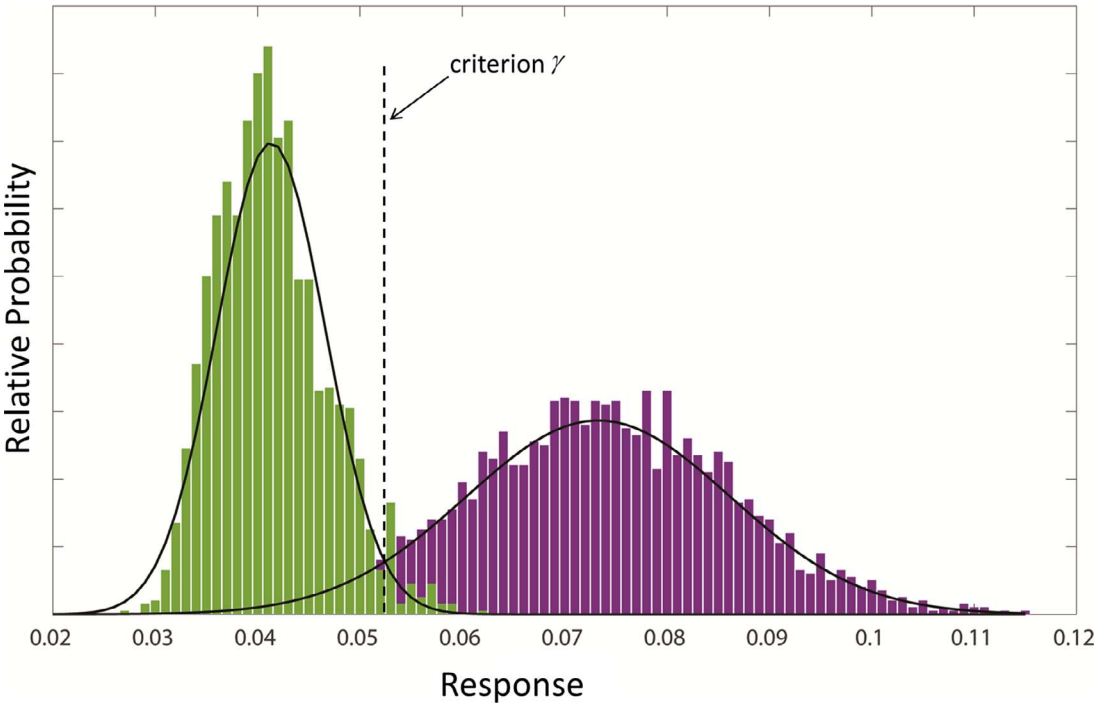

Figure A1. These histograms are responses of a simulated uncertain template matching observer, with an uncertainty radius of 32 pixels. Curves are normal distributions with the same means and standard deviations as the stimulated responses for the two categories (target absent and target present). Detectability is computed from the normal distributions using Equations A1–A3.